Traffic 2006; 7: 308–323
Blackwell Munksgaard

doi: 10.1111/j.1600-0854.2005.00381.x

Vaccinia Virus-Induced Microtubule-Dependent Cellular Rearrangements

Antonino Schepis[1,a], Birgit Schramm[1,a], Cornelis A. M. de Haan[2] and Jacomine Krijnse Locker[1,*]

[1]*European Molecular Biology Laboratory, Cell biology and Biophysics Programme, Meyerhofstrasse 1, 69117 Heidelberg, Germany*
[2]*Virology Division, Department of Infectious Diseases and Immunology, Faculty of Veterinary Medicine, University of Utrecht, Yalelaan 1, 3583 CL Utrecht, the Netherlands*
** Corresponding author: Jacomine Krijnse Locker, krijnse@embl.de*

Although infection with vaccinia virus (VV) is known to affect the cytoskeleton, it is not known how this affects the cellular architecture or whether the attenuated modified VV ankara (MVA) behaves similar to wild-type VV (wtVV). In the present study, we therefore compared effects of wtVV and MVA infection on the cellular architecture. WtVV-infection induces cell rounding early in infection, which coincides with the retraction of microtubules (MTs) and intermediate filaments from the cellular periphery, whereas mitochondria and late endosomes cluster around the nucleus. Nocodazole treatment demonstrates that cell rounding and organelle clustering require intact MTs. At the onset of virus assembly late in infection, cells reflatten, a process that coincides with the regrowth of MTs into the cellular periphery. We find that the actin network undergoes several rearrangements that occur sequentially in time and that closely follow the cell-shape changes. Unexpectedly, these actin changes are blocked or reversed upon nocodazole treatment, indicating that intact MTs are also responsible for the wtVV-induced actin rearrangements. Finally, MVA infection does not induce any of these cellular changes. Because this virus lacks a substantial number of VV genes, MVA opens up a system to search for the molecules involved in wtVV-induced cellular changes; in particular, those that may regulate actin/MT interactions.

Key words: actin, cell shape, microtubules, modified vaccinia virus ankara, vaccinia virus.

Received 29 June 2005, revised and accepted for publication 22 November 2005, published on-line 20 December 2005

Vaccinia virus (VV) is the prototype of the poxviridae, a family of large DNA viruses. Its genome of about 200 kB encodes for more than 250 proteins (1) enabling VV to carry out DNA replication and transcription in the cytoplasm rather than in the cellular nucleus (1). VV is characterized by a complex cytoplasmic life cycle, directed by three classes of genes, early, intermediate and late. Following entry, the viral core is delivered into the cytoplasm, from which a defined set of early mRNAs is transcribed and extruded into the cytoplasm for translation. The early proteins are required to uncoat the viral core and to initiate cytoplasmic DNA replication. Replication sets off the transcription of intermediate and late genes, late proteins being required for virion assembly. During assembly, late in infection, two infectious forms are made; the intracellular mature virus (IMV) and the extracellular enveloped virus (EEV). A small percentage of the intracellular IMVs becomes enwrapped by a double membrane derived from the *trans*-Golgi network (TGN) or endosomes to form the intracellular enveloped virus [IEV (2,3)]. The IEV moves along microtubules (MTs) towards the plasma membrane using the plus-end directed motor protein kinesin-1. Upon fusion of the outer IEV membrane with the plasma membrane, the EEV is released into the extracellular environment. The outer IEV membrane that is fused with the plasma membrane is able to polymerize actin tails, resulting in long filopodia that propel attached EEVs towards neighbouring cells, a process that facilitates cell-to-cell spread of VV (4,5).

VV vaccination was used successfully to eradicate variola virus, the cause of smallpox. Because VV induces an efficient cellular immune response, recombinant VVs are currently tested for their use as live vaccines to protect against other pathogens such as HIV. However, because VV vaccination is accompanied by side-effects, attenuated VV strains, such as modified VV ankara (MVA), are currently preferred. MVA was generated by repeated passaging of the VV strain ankara in chicken embryo fibroblasts (CEFs), resulting in a virus that can make infectious progeny in CEFs and BHK only (6,7). Compared with the wild-typeVV (wtVV) strain Copenhagen, about 65 genes are either deleted or inactive in MVA, accounting for about one third of the genome (8). Immunological studies showed that MVA is able to induce an efficient immune response to recombinant proteins in animals (9,10) and to protect mice and monkeys against lethal doses of poxvirus infections (11,12). Together with the fact that MVA does not cause the side-effects seen upon wtVV infection, it is currently considered a promising candidate to replace wtVV strains in vaccination studies.

To co-ordinate the distinct steps of its complex cytoplasmic life cycle, wtVV interacts with, uses and manipulates many cellular factors. It not only uses membranes and the cytoskeleton but is also able to interfere with signal transduction, because wtVV activates extracellular signal regulated kinase cascade and inhibits Stat1 activation (13,14). Moreover, wtVV has several strategies to inhibit apoptosis

[a]These authors contributed equally to this work.

and to evade the immune system (15–18). WtVV infection also affects host functions and metabolism, as it inhibits for instance host RNA and protein synthesis (19,20). The complex way wtVV interacts with the host cell to coordinate the distinct steps of its life cycle, is known to lead to pronounced changes in cell morphology, collectively called cytopathic effect (21). Changes in cell shape and size are likely correlated with rearrangements of the host cytoskeleton, known to occur during wtVV infection. It has been shown, for instance, that the actin cytoskeleton is extensively modified both early and late in infection (22,23). WtVV is also known to interfere with the organization of MTs and intermediate filaments (24,25). In contrast, relatively little is known about cytopathic effects induced by MVA infection. In HeLa cells, MVA assembly is blocked at late stage of infection; immature virions (IVs), the precursors of the IMV, are made, which fail to assemble into infectious IMVs, whereas the stages preceding IV formation occur normally and with the same efficiency compared to wtVV (26). Recent data suggested that, late in infection in HeLa cells, MVA affects the cell shape differently from other VV strains, suggesting that MVA infection has a different effect on the host cytoskeleton (27).

Given the increasing interest in MVA as a putative live vaccine, we decided to systematically compare effects of wtVV and MVA infection on the cellular architecture. For this, we used a synchronized infection system to compare in detail by light microscopy possible changes to the cytoskeleton and the intracellular distribution of organelles. We find that wtVV infection extensively modifies the cell shape and size, the cytoskeleton as well as the intracellular distribution of mitochondria and late endosomes. These changes come in two subsequent phases that closely match the early and late stages of the viral life cycle. Importantly, none of these changes are seen upon infection with MVA, implying that this virus misses the wtVV factor(s) that induces these cellular changes.

Results

WtVV infection induces reversible cell rounding in an MT-dependent manner

Throughout this study, cellular changes induced by wtVV infection will be described and analyzed in a quantitative manner, and we therefore used conditions to synchronize the infection. The use of purified, monodisperse virus preparation and relatively short infection times (15–20 min) were sufficient to obtain this goal (see *Supplementary information 1* available online at http://www.blackwell-synergy.com). Western-reserve strain of VV was used and for purposes of this study is termed wtVV. Throughout all experiments, wtVV was compared to the attenuated VV strain MVA, and all of the cell changes described below were seen in both HeLa and PtK2 cells.

WtVV is known to induce cell rounding early in infection in a variety of cells, which appeared to be dependent on the synthesis of early viral proteins (20). Consistently, Hela (as well as PtK2; not shown) cells infected for 2.5 h with wtVV showed a rounded morphology, apparently loosing cell–cell contacts. MVA infection, in contrast, did not result in cell rounding as the cells remained flat and did not loose cell–cell contacts (Figure 1A–C). To obtain a quantitative impression of the cell rounding, the surface occupied by the cell on the coverslip (which is further referred to as 'cell surface' or 'cell size') was estimated over the course of infection with wtVV or MVA and compared to uninfected control cells. As early as 2.5 h post-infection wtVV-infected cells occupied about 40% less surface on the coverslip than uninfected controls, an effect that was reversed late in infection, because, at 8.5 h, infected cells had regained the same size as uninfected control cells (Figure 1D). Surprisingly, MVA-infection resulted in a reversible increase in cell surface that was most prominent at 4.5 h post-infection (Figure 1D).

As cell size and shape are intimately linked to the cytoskeleton, we asked whether MTs played a role in cell rounding using the MT depolymerizing drug nocodazole. Whereas nocodazole treatment did not significantly affect the size of uninfected cells, it efficiently blocked cell rounding induced by wtVV infection (Figure 1E). Furthermore, when nocodazole was added at 2.5 h post-infection, when infected cells were already rounded, cells reflattened, collectively demonstrating that intact MTs were responsible for cell rounding (not shown). A detailed morphological analysis of the MT network during the course of infection will be described below.

Thus, whereas wtVV infection results in reversible and MT-dependent cell rounding early in infection, MVA infection induced an increase in cell surface, which was also reversible.

Intermediate filaments collapse during VV infection

Intermediate filaments are known to be affected upon VV infection (24). Indeed, upon infection with wtVV, the vimentin-positive network retracted around the nucleus (Figure 2C,F), changes that were not seen upon infection with MVA (Figure 2B,E). When measuring the relative distribution of vimentin over the course of infection (see *Materials and Methods*), which was typically 70–80% in uninfected control cells, this percentage was clearly reduced upon wtVV infection (Figure 2G). The vimentin distribution displayed a certain pattern during the course of infection, similar to the change in cell shape. The collapse was most prominent at 4.5 h postinfection with a relative distribution of intermediate filaments of about 40% of the total cell surface. At late times (8.5 h) post-infection, the vimentin collapse was reversed to some extent but intermediate filaments did not regain the distribution seen in uninfected cell (Figure 2G). Similar measurements of MVA-infected cells showed that the relative

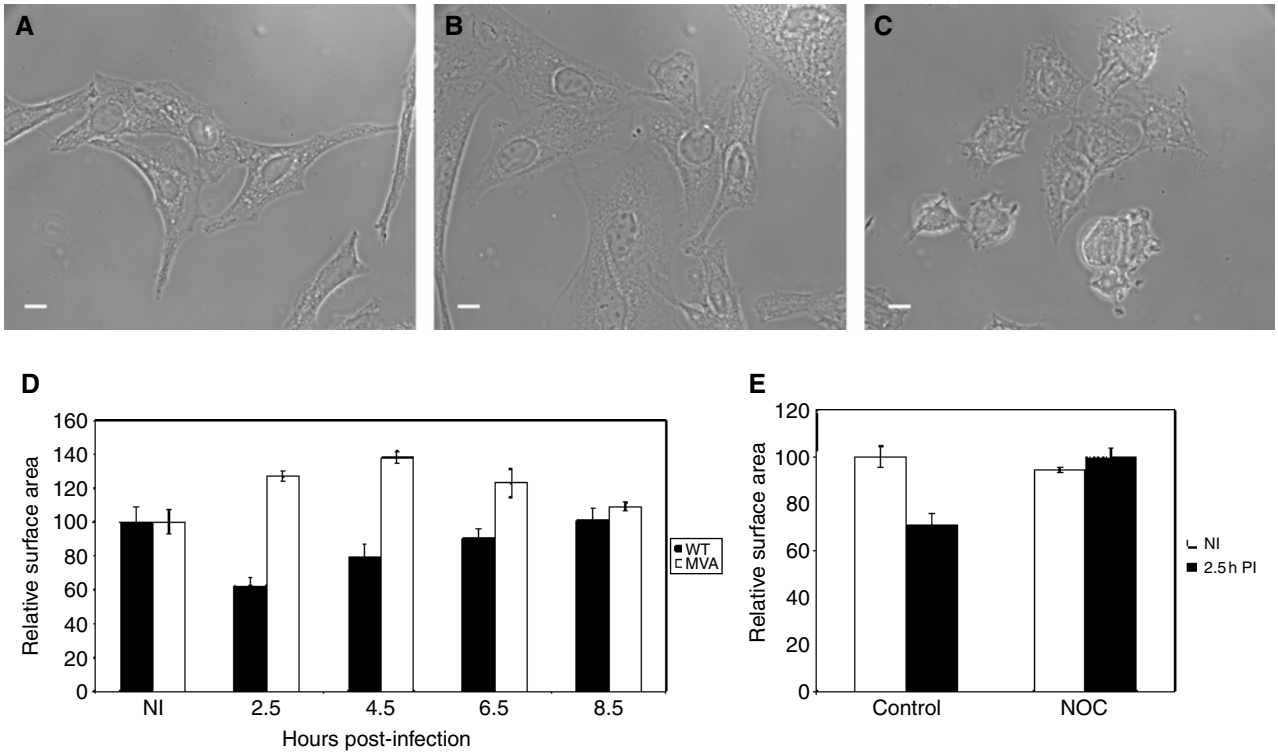

Figure 1: VV infection induces reversible and MT-dependent cell rounding. In (A–C), DIC images of HeLa cells left uninfected (A) or infected for 3 h with MVA (B) or wtVV (C). WtVV-infected cells round up and loose cell–cell contacts. In (D), the surface area of cells (defined as the surface occupied by the cell on the coverslip) was calculated at the indicated times postinfection with wtVV (WT) or MVA. The relative surface area of wtVV or MVA-infected cells was calculated by dividing the average surface area of 50 cells by the average surface of uninfected cells (NI) and by taking uninfected cells as 100%. The data represent the average and standard deviations of 50 cells sampled on three different coverslips. In (E), cells were treated (NOC) or not (control) with 20 μM nocodazole before wtVV infection, and the relative surface area was measured at 2.5 h postinfection as in (D) taking uninfected control cells as 100%. Bars 10 μm.

distribution of intermediate filaments was unchanged compared to uninfected control cells (not shown).

Thus, intermediate filaments collapsed around the nucleus early in wtVV infection, and this effect was partially reversed at later times.

Mitochondria collect around the nucleus

Using organelle-specific markers in HeLa and PtK2 cells, we next tested whether the intracellular distribution of membrane compartments was also affected upon wtVV infection. We typically found that mitochondria and late endosomes (see below) displayed a significantly altered cytoplasmic distribution in wtVV-infected cells.

Upon wtVV but not MVA infection, mitochondria clustered around the nucleus early in infection (Figure 3A–F). When the relative distribution of the mitochondrial labelling was quantified in the same manner as the vimentin labelling, mitochondria occupied 60–70% of the total cell surface in uninfected cells, and this percentage was clearly reduced upon wtVV infection (Figure 3G). The wtVV-induced collapse was completely reversed late in infection, because at 8.5 h, the relative distribution of mitochondria was similar to uninfected control cells (Figure 3G). Furthermore, the collapse appeared to depend on MTs, as nocodazole entirely prevented the clustering of mitochondria (Figure 3G).

Thus, mitochondria cluster around the nucleus in a reversible, MT- and time-dependent manner.

Late endosomes cluster around the nucleus in an irreversible manner

In uninfected HeLa cells, late (lamp-1 positive) endosomes appear as punctate structures distributed over the cytoplasm (Figure 4A,D). In addition, in some cells, a subset of the late endosomes cluster on one side of the nucleus (not shown). Upon infection with wtVV, but not MVA, the dispersed endosomal pattern found in the majority of uninfected cells was entirely lost. Instead, over time, late endosomes coalesced into one spot next to the nucleus, in the majority (around 70%) of the wtVV-infected cells (Figure 4C,F). The remaining 25–30% of the cells displayed a pattern, in which a subset of the endosomes clustered around the nucleus, in a way similar to the second pattern seen in control cells. The endosomal pattern was then classified in three categories; the dispersed

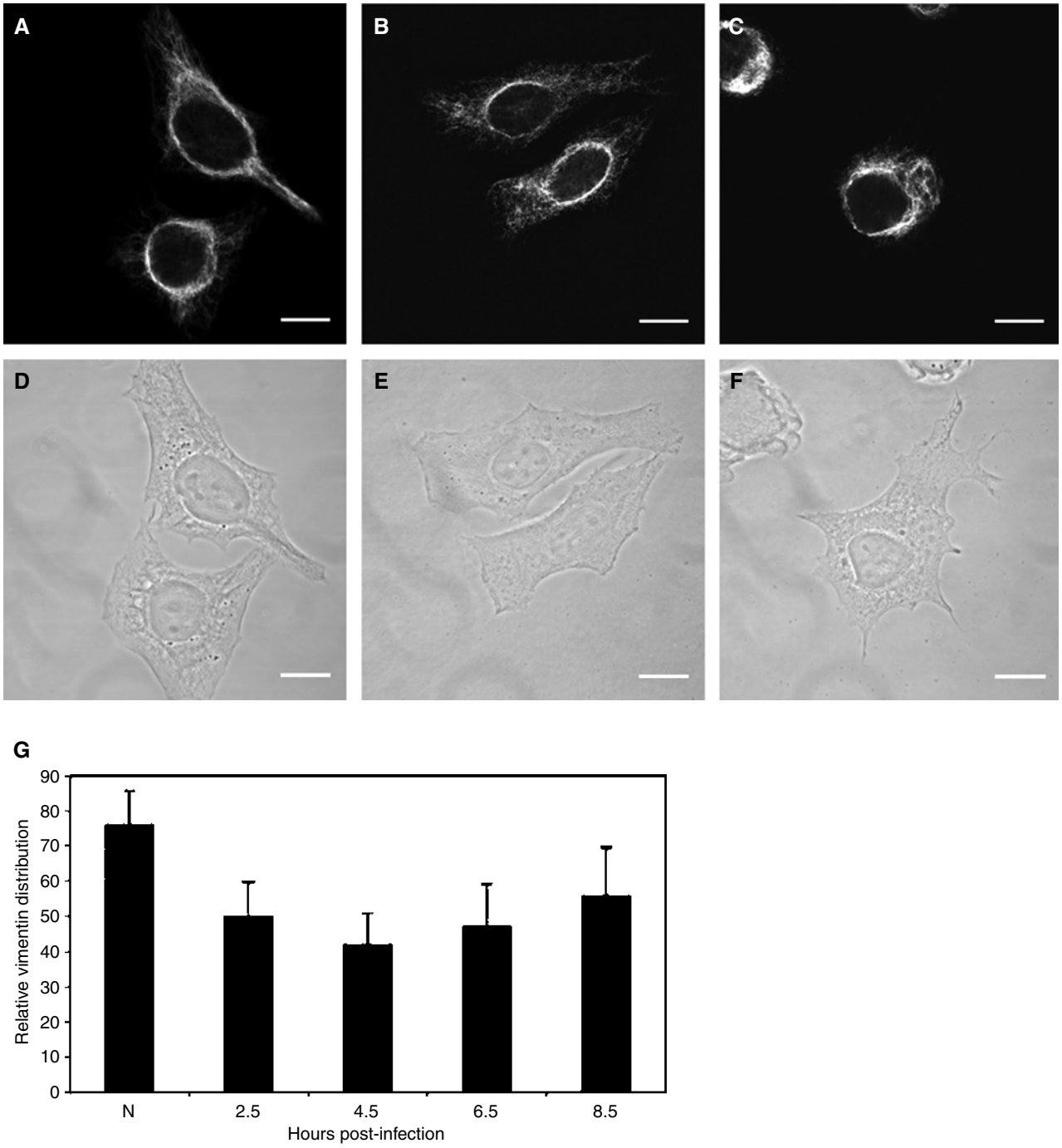

Figure 2: Intermediate filaments cluster around the nucleus upon VV infection. In (A–C), confocal images of HeLa cells left uninfected (A) or infected for 4 h with MVA (B) or wtVV (C) labelled with anti-vimentin followed by anti-mouse coupled to Cy-3. WtVV infection induces clustering of intermediate filaments around the nucleus (C). (D–F) are the corresponding DIC images. Note that the cell shown in (F) is from 4 h postinfection and thus appears less rounded than the cell in Figure 1C which is from 3 h postinfection. In (G), the relative surface occupied by the vimentin labelling upon wtVV infection, was calculated by relating the area occupied by the antibody labelling to the total cell surface (defined by the area of the cell occupied on the coverslip) which was set at 100%. The data represent the average percentage and standard deviations derived from 70 cells per time point. NI-uninfected cells. Bars 10 μm.

pattern seen in the majority of the uninfected cells, the intermediate pattern displaying some peri-nuclear accumulation (defined as semi-dispersed), whereas a clustered phenotype defined the pattern seen in the majority of the wtVV-infected cells (Figure 4A–F). A dispersed pattern was seen in 70% of the uninfected cells (or in MVA-infected cells; not shown), with 30% being semi-dispersed (Figure 4G), whereas a clustered phenotype was never

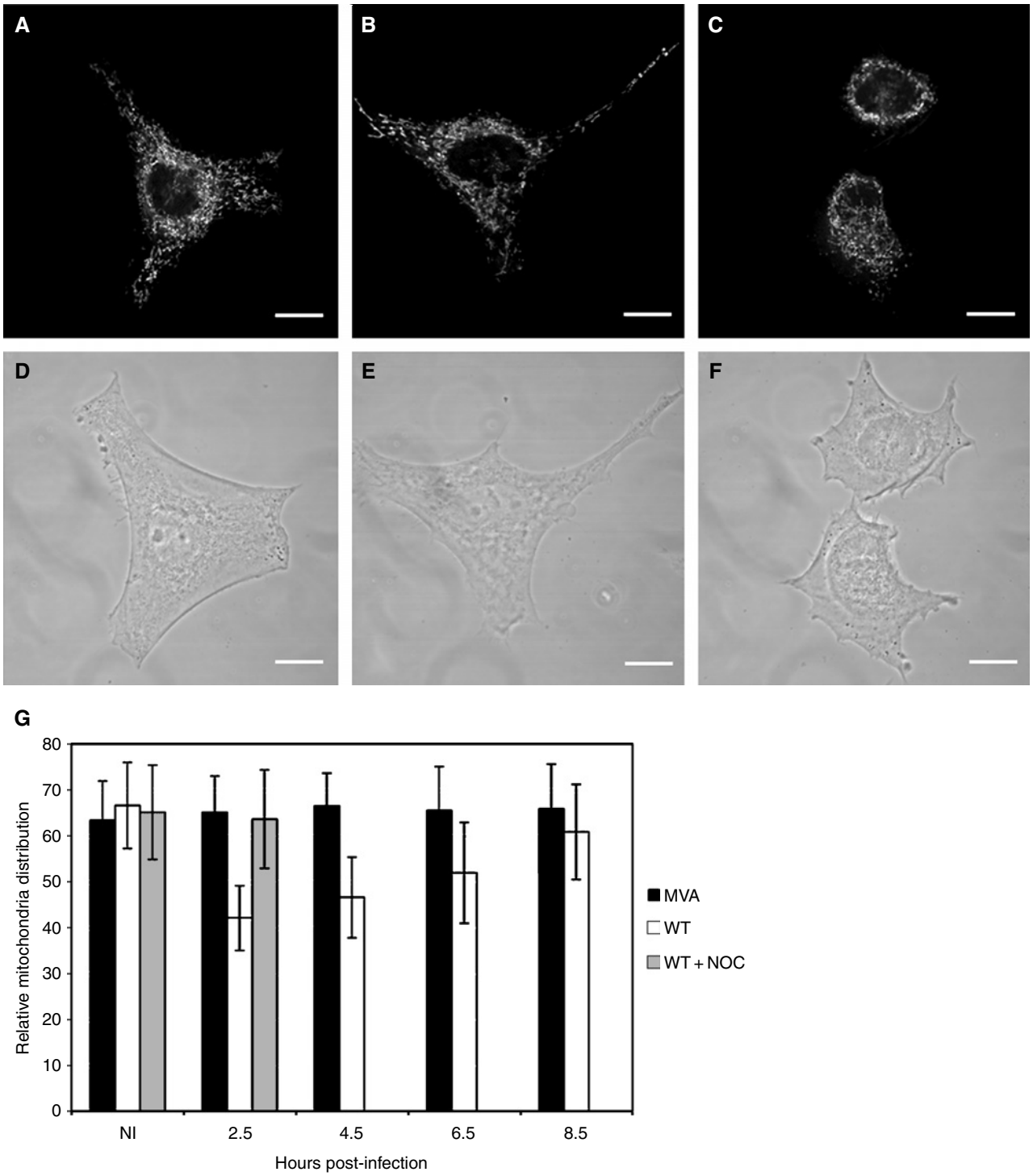

Figure 3: VV infection induces reversible clustering of mitochondria around the nucleus. In (A–C), confocal images of HeLa cells left uninfected (A) or infected for 4 h with MVA (B) or wtVV (C). Mitochondria were labelled by adding 300 nM mitotracker to the cells 30 min before fixing. Whereas in uninfected and MVA-infected cells mitochondria are spread over the cytoplasm, upon wtVV infection, they cluster around the nucleus. (D–F) corresponding DIC images. In (G), the relative distribution of mitochondrial labelling was calculated as described in Figure 2 for vimentin of uninfected cells (NI), cells infected with MVA or infected with wtVV (WT). To evaluate the role of MTs, we added to one set of cells, nocodazole at 20 μM before infection and the relative distribution of mitochondria measured at 2.5 h postinfection (WT + NOC). Shown here is only the 2.5 h time point, but similar results were obtained at all times postinfection. NI-uninfected cells. Bars 10 μm.

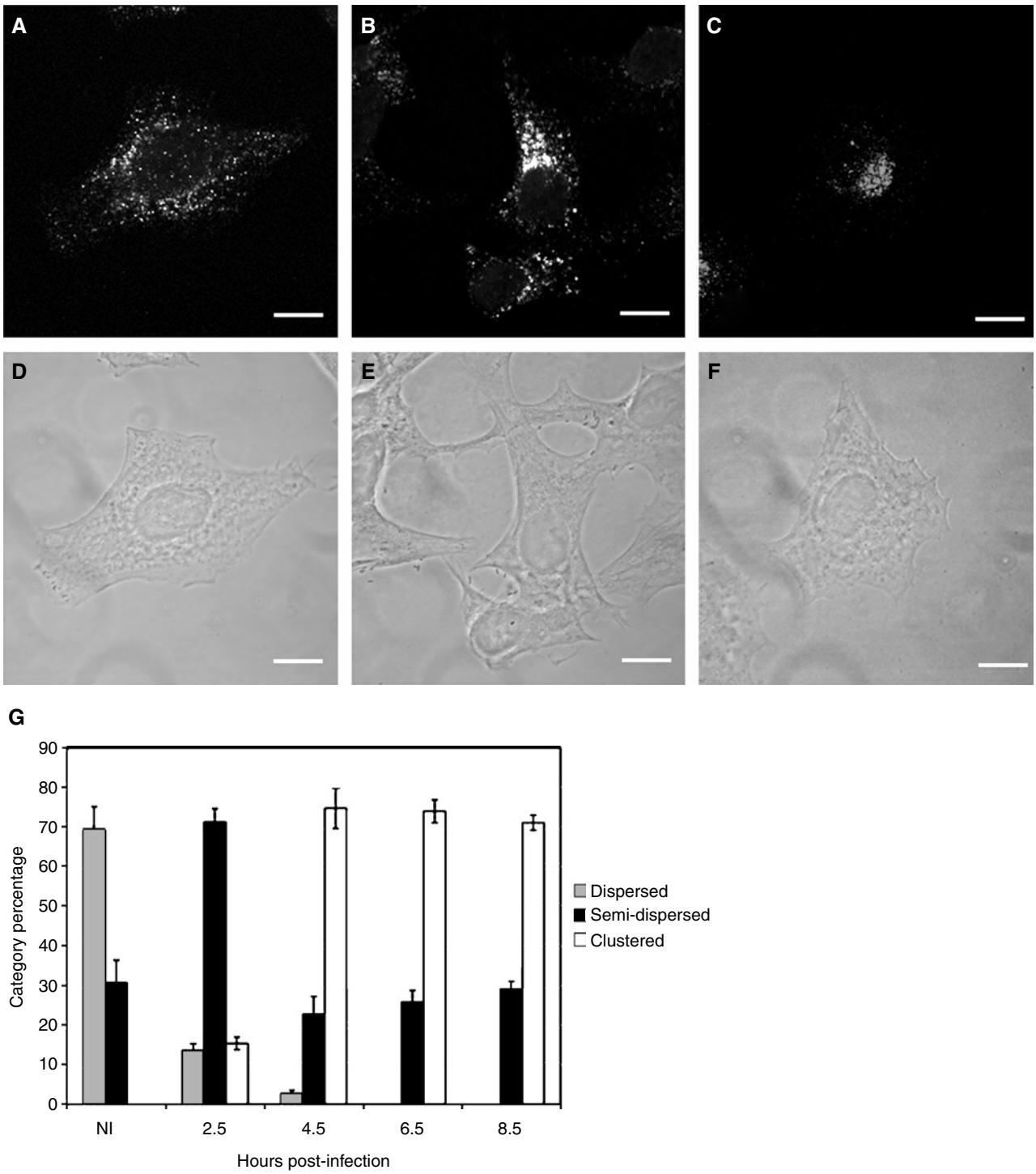

Figure 4: Late endosomes cluster irreversibly around the nucleus. In (A–C), confocal images of HeLa cells left uninfected (A) or infected for 4 h with MVA (B) or wtVV (C). Fixed cells were labelled with a monoclonal antibody to lamp-1, followed by anti-mouse coupled to Cy-3. In uninfected cells or upon MVA infection, late endosomes display a dispersed pattern, whereas in VV-infected cells, endosomes cluster close to the nucleus. (D–F) corresponding DIC images. In (G), the endosomal pattern was classified in three categories, as described in the text, the pattern seen in (A) and (B) was defined as dispersed, the VV-induced phenotype shown in (C) as clustered. Intermediate patterns were defined as semi-dispersed. Per indicated time postinfection 100 cells were classified according to these three categories. The data represent the average percentage and standard deviation (derived from two independent experiments) of each category observed under each of the different conditions and times post-infection. Bars 10 μm.

observed. Upon wtVV infection, the dispersed pattern gradually disappeared. From 4.5 h post-infection onwards, about 70% of the infected cells displayed a clustered phenotype, with 30% semi-dispersed (Figure 4G). Again, the endosomal collapse was inhibited by nocodazole, implying that it depended on intact MTs (not shown). In contrast to the cellular changes described above, the wtVV-induced pattern was not reversed late in infection, and thus, late endosomes collapsed around the nucleus in an irreversible manner (Figure 4G).

The actin network undergoes several distinct changes during the infectious cycle

Previous studies showed that wtVV infection induces the disappearance of actin fibres early in infection (22) and the rearrangement of the actin network late in infection, concomitant with the formation of virus-tipped actin tails (23). The actin pattern was therefore followed over the time of infection using synchronized infection conditions. PtK2 were used in the next set of experiments, because these cells are well suited to follow distinct actin and MT patterns.

In uninfected PtK2 cells, the actin network appeared as fibres that crossed the entire cellular cytoplasm (Figure 5A), a pattern that remained mostly unaffected upon infection with MVA (Figure 5B–E). Upon infection with wtVV, the actin network displayed four different patterns that appeared sequentially during the infection. At 2.5 h post-infection, the actin pattern, typically seen in uninfected cells, had largely disappeared, and instead, actin outlined the cell borders (Figure 5F; cells marked with '1' in Figure 5F,G are indicated as a typical example). In a subset of cells, actin was furthermore concentrated on one side of the cell, displaying a lamelipodia-like protrusion (Figure 5G, cells indicated with '2'), a pattern that was most prominently seen around 4.5 h post-infection (Figure 5G,K). From about 6.5 h post-infection, the early actin pattern was gradually replaced by two other phenotypes; in a subset of cells, actin appeared as thin fibres that crossed most of the cellular cytoplasm (Figure 5H,I indicated with '3'). Cells with this actin pattern had typically adopted a stellate, rather than a rounded, morphology. Finally, at late times post-infection (8–10 h), some cells formed multibranched protrusions outlined by thin actin borders, with no F-actin staining in the central region of the cell (Figure 5J, '4'). Figure 5K shows the relative distribution of the different actin patterns marked 1–4 on the light microscopy images in Figure 5F–J over the time of infection. As exemplified by the images F–J, wtVV-infected cells first displayed an early peripheral actin pattern which appeared polarized in a subset of cells, which was then replaced by two different patterns that appeared later in infection. We believe that the coexistence of at least two different actin phenotypes both early and late in infection reflects the dynamic nature of actin or perhaps different cellular states.

Concomitant with the actin changes, wtVV infection resulted in rearrangements of focal complexes. Generally, focal adhesion sites (assessed by anti-vinculin and anti-paxillin labelling) decreased in number and concentrated at the cell borders where actin was also concentrated (*Supplementary information 2* available online at http://www.blackwell-synergy.com).

Thus, the actin cytoskeleton undergoes dramatic rearrangements during the course of infection that apparently coincide with the changes in cell shapes and that seemingly followed distinct steps of the virus life cycle (summarized in Figure 9). As all of the wtVV-induced changes described above depended on MTs (Figures 1E and 3G and data not shown), we next investigated to what extent the actin rearrangements depended on intact MTs.

VV-induced actin rearrangements require intact MTs

The actin changes described above closely matched the cell shape changes, suggesting that these were driven by the actin rearrangements rather than the MT network. We therefore tested, using nocodazole, to what extent the actin changes depended on intact MTs. In cultured cells, nocodazole treatment does not significantly affect the viral life cycle. Whereas this drug reduces early transcription and early protein synthesis about twofold (28), DNA replication is not significantly affected nor is the synthesis of viral late proteins and the production of infectious progeny (our unpublished results described in *Supplementary information 1* available online at http://www.blackwell-synergy.com). TGN wrapping and IEV formation are, however, strictly dependent on intact MTs (25, see *Discussion*).

When cells were treated with nocodazole before infection and fixed at either 3 or 8 h post-infection with wtVV, the actin changes typical of these times of infection were not seen (Figure 6A–D). Instead, the actin network looked similar to uninfected control cells. Moreover, if infected cells were subjected to nocodazole treatment at times when the actin network was already rearranged, an actin pattern similar to uninfected cells reappeared (not shown). Similarly, upon nocodazole washout, the actin network was rearranged into the pattern similar to untreated/VV-infected cells (not shown), collectively showing that the actin rearrangements could be induced or reversed depending on the presence or absence of MTs, respectively.

Together these data imply that intact MTs are required to induce the actin rearrangements seen upon wtVV infection.

MTs undergo two consecutive changes during the course of VV infection

Our collective data showed that MTs played a crucial role in all of the cellular changes, and the morphology of the MT network was therefore studied next. WtVV-induced changes to the MT network were described before (25),

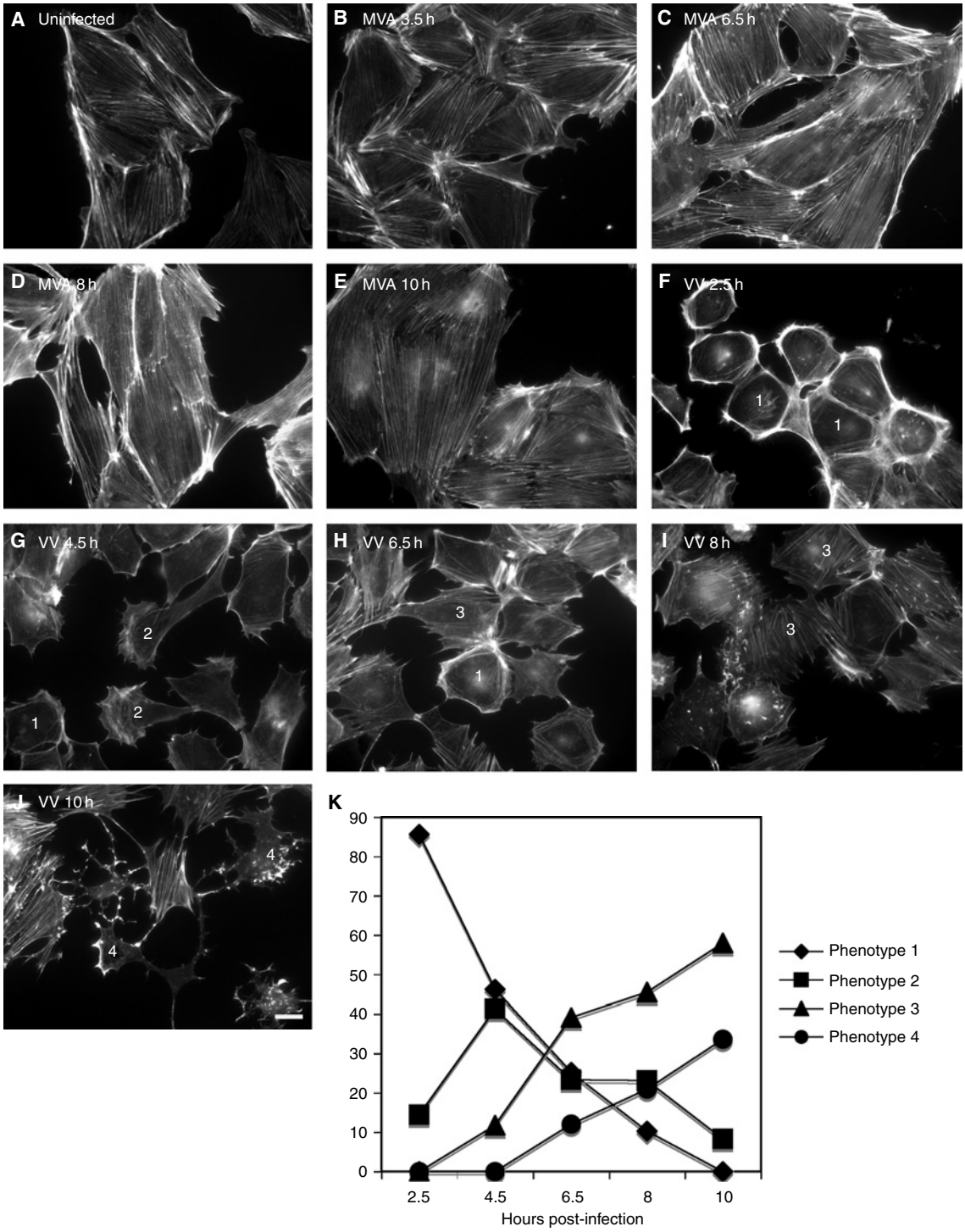

Figure 5: Actin rearrangements during the course of infection. A uninfected PtK2 cells, (B–E) PtK 2 cells infected for 3.5 h (B), 6.5 h (C), 8 h (D) or 10 h (E) with MVA. (F–J) PtK2 cells infected with wtVV, fixed at 2.5 h (F), 4.5 h (G), 6.5 h (H), 8 h (I) and 10 h (J) post-infection and labelled with phalloidin rhodamine. Central actin fibres disappear early in infection (F, example indicated with '1'), and actin appears as peripheral fibres, sometimes polarized towards one cell end (G, '2'). At later times central fibres reappear (H and I, '3'). Some cells form multibranched protrusions (J, '4'), in which actin aligns the cell borders as a thin rim. In (K), the different actin patterns marked 1–4 on the images in (F–J) were quantified over the time of infection. Per time point of infection, 100 cells were classified into each of the four actin phenotypes indicated in the images (F–J). The graph represents the percentage of each phenotype (indicated as phenotype 1–4 in the legend to the graph) that occurs at the indicated times postinfection. Bar in J 10 μm. It should be noted that all images are represented at same magnification. The cell size differences, most obviously seen when comparing MVA infection to wtVV infection, are thus a direct representation of cell rounding or reflattening induced by wtVV.

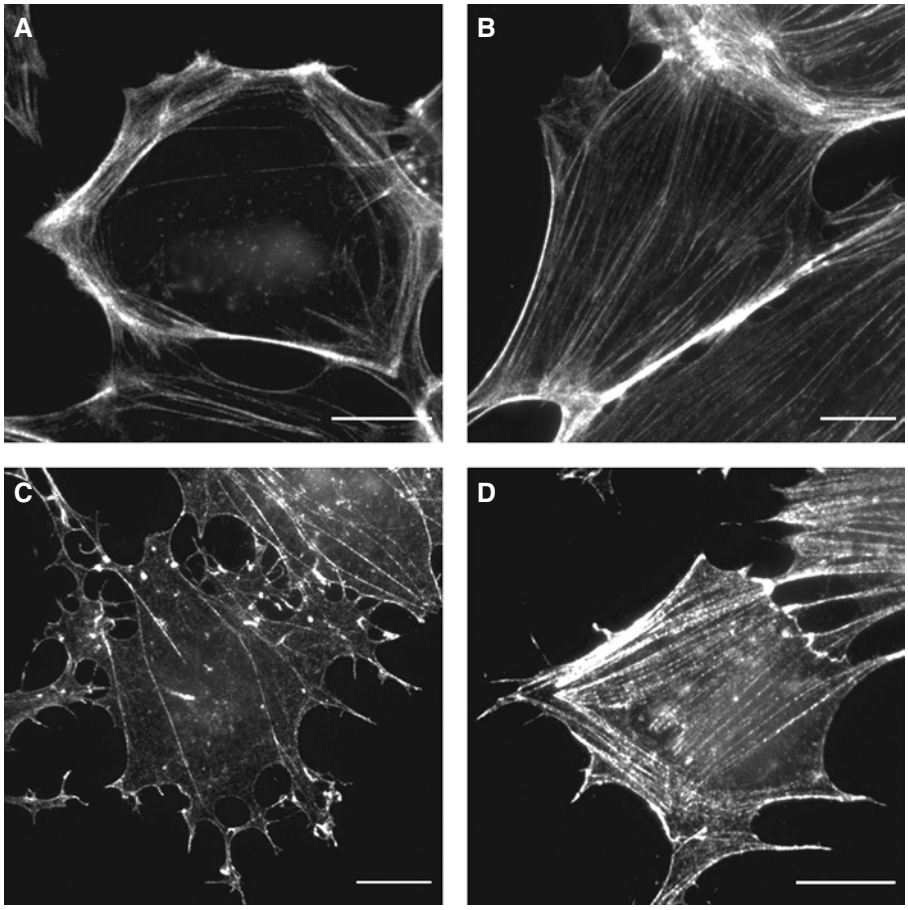

Figure 6: Actin is rearranged in a MT-dependent fashion. PtK2 cells were left untreated (A and C) or treated (B and D) for 60 min on ice with 30 μM nocodazole followed by 60 min at 37 °C before infection with wtVV and fixation at 3 h (A and B) and 8 h (C and D) post-infection. The cells were labelled with phalloidin coupled to rhodamine. Bars 10 μm.

but these results were not obtained under synchronized infection conditions and were not compared to MVA infection.

In uninfected PtK2 cells, MTs emanate from one point [Microtubule Organising Centre (MTOC)] close to nucleus and are distributed throughout the entire cytoplasm. At the cell cortex, individual MT tracks are often seen to bend, apparently following the plasma membrane along actin filaments (Figure 7B, see also inset). This pattern was not dramatically altered upon infection with MVA (Figure 7G,H). WtVV infection, however, induced prominent changes to the MT network. As early as 1 h post-infection, the MT network started to retract from peripheral regions of the cell (not shown), a phenotype that was most prominently seen around 4.5 h post-infection (up to 40% of infected cells) (Figure 7D). The MT retraction was readily seen when cells were labelled with anti-EB1, a MT plus-end-binding protein (29,30), suggesting a specific retraction of the dynamic plus ends of MTs (compare Figure 7A–C). The MT-retracting phenotype consisted of a combination of MT bundling, a general MT disorganization, unusual MT-curling and the shortening of (peripheral) MT tracks (Figure 7D, see also inset). Furthermore, the cellular periphery that was free of MTs was filled instead with actin fibres described above, occasionally contacted by individual MT tracks (Figure 7D and inset). Concomitant with further changes in cell shape (spiky morphology, see above) that became prominent from 6 h postinfection onwards, the MT network underwent a second phase of rearrangement. MTs reached out into the peripheral regions, specifically feeding into the stellate-like extensions and into the long and multi-branched protrusions that typically appeared at 8–10 h post-infection (Figure 7F). In these protrusions, individual MT tracks apparently contacted actin filaments that aligned the plasma membrane (Figure 7F, see also inset). In such filopodia, EB1 labelling specifically highlighted the MT tips, suggesting an enrichment of dynamic plus ends in the plasma membrane protrusions (Figure 7E). The overall organization of the MT network did, however, not regain the morphology seen in uninfected cells; MTs remained mostly unorganized, seemingly not properly focused at the MTOC.

Thus, MTs undergo an apparent retraction early in infection coinciding with cell rounding, whereas later during the cell-reflattening phase, they regrow towards the cellular periphery.

A subset of MTs resist nocodazole de-polymerization

The curled/retracted MT phenotype seen early in infection could be the results of the increased binding of MT-associated

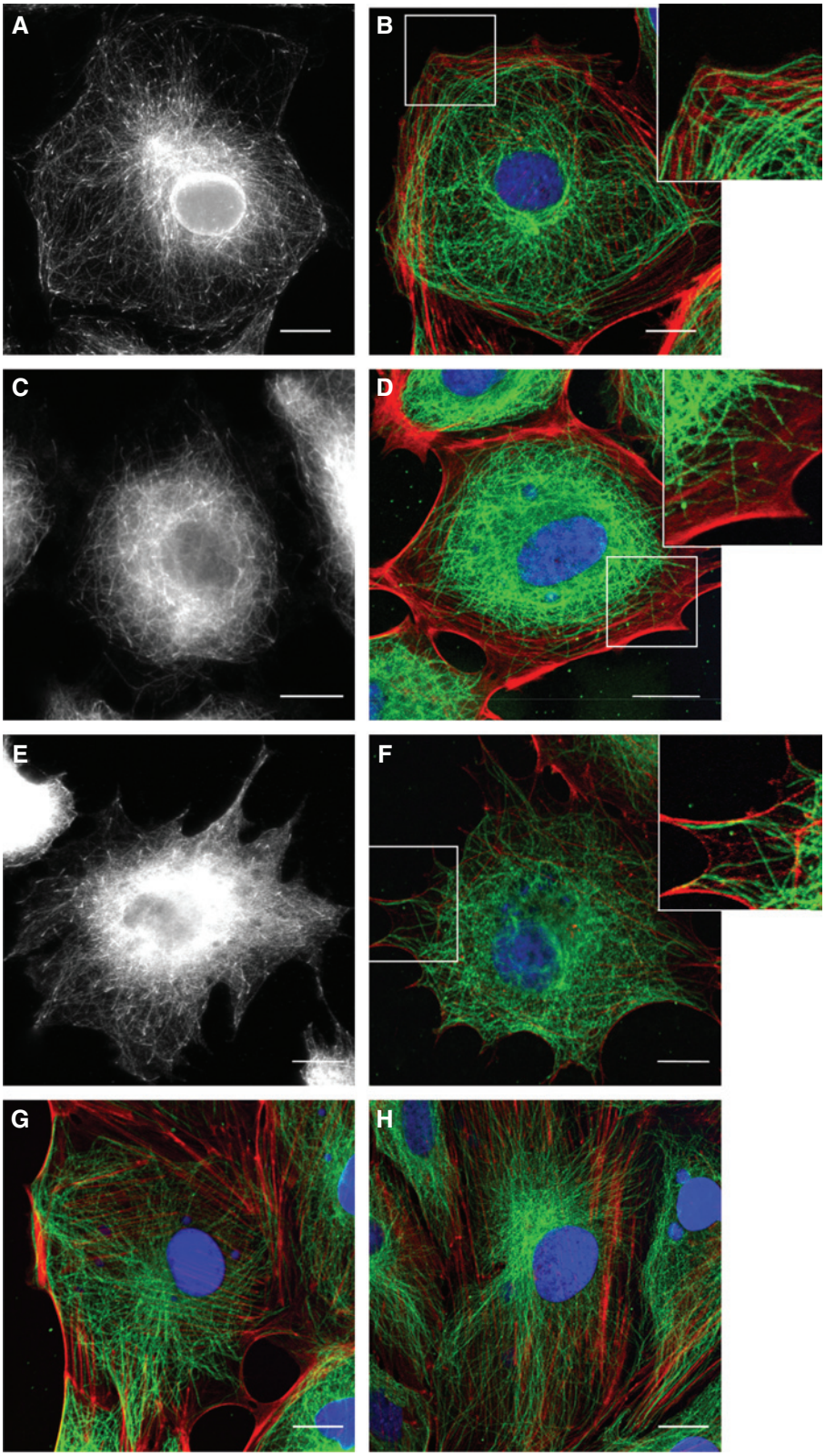

Figure 7: Rearrangements of MTs during the course of infection. PtK2 cells were left uninfected (A and B) or were infected for 4.5 h (G) and 8 h (H) with MVA or 4.5 h (C and D) and 8 h (E and F) with wtVV before fixation. A, C and E were fixed with methanol and labelled with anti-EB1, followed by anti-rabbit coupled to Cy3. B, D, F, G and H were fixed with PFA and triple-labelled with anti-tubulin (green), phalloidin coupled to rhodamine (red) and Hoechst (blue). The insets in B, D and F correspond to the boxed areas. Bars 10 μm.

proteins (MAPs), leading to MT stabilization, as suggested by Ploublidou *et al.* (25). To obtain an impression whether wtVV infection altered MT dynamics, we pretreated cells with nocodazole prior to infection. MT-depleted cells were then infected and pre-extracted with Triton-X-100 before fixation at 3 or 8 h post-infection.

Uninfected or MVA-infected cells revealed about one to three MT filaments that resisted nocodazole treatment (Figure 8A,B). The latter were also seen upon VV infection (not shown), but additionally many small MT pieces were observed both early (Figure 8C) and late (not shown) in infection. Identical results were obtained if infected cells were treated with nocodazole after infection, suggesting that, upon VV infection, a subset of MTs became resistant to nocodazole de-polymerization. We used a panel of antibodies to both cellular and viral proteins and asked whether these proteins localized to the nocodazole-resistant MT pieces. Both early and late in infection, the nocodazole-resistant MT pieces were not decorated with any of the antibodies to viral proteins tested [the early proteins I3L and H5R and the late proteins A10L and L4R (not shown)]. They did contain a subset of known cellular MAPs, such as the plus-end-binding proteins EB-1, Clip-170, $p150^{glued}$, as well as γ-tubulin (not shown).

Thus, wtVV infection, but not MVA infection, induces the formation of a subset of MTs that resist nocodazole treatment, which may reflect the ability of wtVV to stabilize MTs (see *Discussion*).

The role of VV-early and -late protein synthesis

The above results showed that the cellular changes induced by wtVV infection displayed two phases. Early in infection, cells rounded up, concomitant with the clustering of organelles around the nucleus and changes to the cytoskeletal network. Late in infection, most of these phenotypes were partially or completely reversed. The addition of cycloheximide (CX) added before or immediately after infection allows viral binding and entry but not the synthesis of VV-early proteins. In contrast, hydroxyurea (HU) blocks viral replication and as a consequence late, but not early, protein synthesis. These two drugs were used to test whether the synthesis of VV early or late proteins correlated with the two phases of the observed changes.

To address the role of wtVV-early proteins in the early phenotypes, we treated cells 15 min prior to infection with either CX or HU, fixed at 3–3.5 h post-infection. CX efficiently blocked all of the early VV-induced changes (Table 1). These included the changes to the cytoskeleton, the MT retraction and the appearance of nocodazole-resistant MT-pieces, the actin and intermediate filament rearrangements and cell rounding. Furthermore, CX prevented the clustering of mitochondria and late endosomes. In the presence of HU, however, all these changes occurred to the same extent as without drugs (Table 1), showing that wtVV-early protein synthesis was required and sufficient to induce the 'early' phenotypes.

To test whether the synthesis of late proteins was required to reverse these phenotypes, we added HU immediately after infection to block late wtVV protein synthesis and cells fixed at 8.5 h post-infection. In the continued presence of HU, the cells remained small, and mitochondria and intermediate filaments remained clustered around the nucleus (Table 1). Compared with 2–4 h post-infection without HU, we did observe subtle rearrangements of the actin and MT network upon prolonged incubation with HU. MTs appeared to regrow into the cellular periphery, the cells gained a more spiky morphology, and the prominent actin bundles disappeared from the cellular rims. HU, however, efficiently blocked the extreme stellate morphology characterized by long multibranched protrusions and disappearance of actin filaments seen late in infection (8–10 h post-infection) without the drug.

These results show that, whereas the synthesis of VV-early proteins is required and sufficient to induce cell

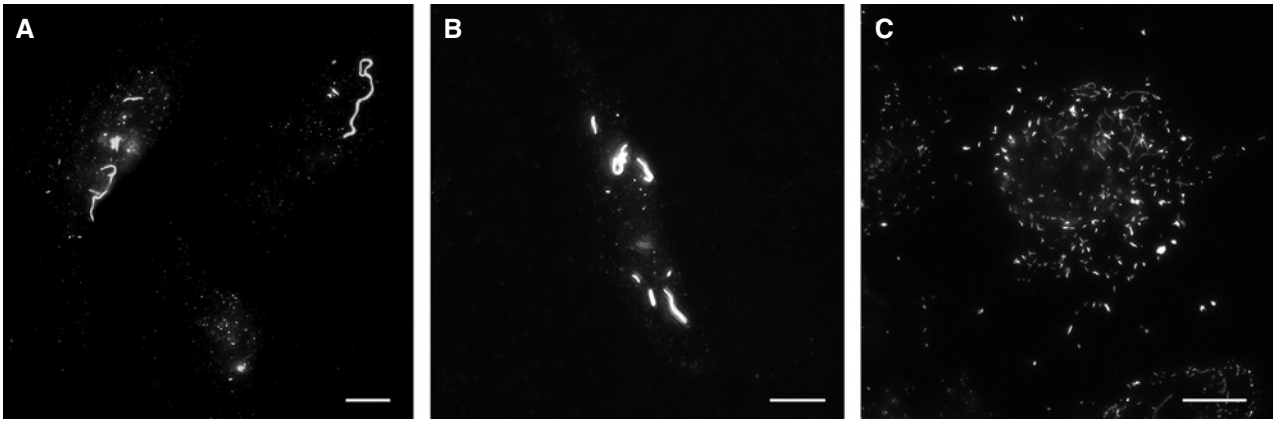

Figure 8: VV infection induces the formation of nocodazole-resistant MT pieces. HeLa cells pretreated with nocodazole as described for Figure 6 and mock infected (A) or infected with MVA (B) or wtVV (C). At 3 h post-infection, cells were pre-extracted with Triton-X-100 before fixation and labelled with anti-tubulin. In uninfected and MVA-infected cells anti-tubulin reveals several long MT fragments that apparently resist nocodazole treatment. WtVV infection results in many short tubulin-positive MT pieces. Bars 10 μm.

Table 1: Overview of the cellular changes induced by wtVV and effects of cycloheximide and hydroxyurea

Cellular phenotype[a]	Control[b]	3.5 h p.i.	CX 3.5 h[c] p.i.	HU 3.5 h[c] p.i.	Control[b]	8h30 p.i.	HU[d] 8.5 h p.i.
Early peripheral actin pattern	No	Yes	No	Yes	No	No	No
MT retraction	No	Yes	No	Yes	No	No	No
MT stabilization	No	Yes	No	Yes	ND	Yes	ND
Vimentin distribution	74%	50%	69%	49%	72%	56%	ND
Mitochondria distribution	68%	43%	68%	45%	66%	62%	48%
Late endosome clustering	0%	75%	0%	73%	0%	75%	ND
Cell surface	100%	68%	95%	71%	100%	103%	72%

[a]Cellular phenotype refers to the cellular changes induced by wtVV infection as described in the text. For the categories early peripheral actin pattern, MT retraction and MT stabilization (the appearance of nocodazole-resistant MT pieces), 'yes/no' indicates whether or not these phenotypes were observed under the indicated conditions. The percentages for the remaining phenotypes (distribution of vimentin, mitochondria, late endosomes and the changes in cell surface) represent measurements identical to those shown in Figure 1D (surface area) or Figures 2G, 3G and 4G (distribution of vimentin, mitochondria and late endosomes, respectively). Except for the actin and MT changes, for which PtK2 cells were used, all other phenotypes were evaluated in HeLa cells. ND, not done.
[b]Control is uninfected HeLa or PtK2 cells fixed at 3.5 h or 8.5 h post-infection (p.i.). To estimate the cell surface changes, we took uninfected cells as 100%. Late endosome clustering refers to the percentage of cells displaying clustering of late endosomes close to the nucleus.
[c]To test for a role of early VV protein synthesis in the early phenotypes, we added CX (25 μg/mL) or HU (5 mM) immediately after infection and the cellular phenotypes estimated as described in the text.
[d]To test for a role of late VV protein synthesis, HU was added immediately after infection and the cells fixed at 8.5 h post-infection.

rounding and organelle clustering, the synthesis of wtVV-late proteins is required to reverse most of these effects.

Discussion

The role of MTs

The present study was aimed at comparing systematically the possible cellular changes that occur upon infection with wtVV and MVA. Using a synchronized infection, we show that wtVV infection first induces cell rounding and then reflattening, processes that coincided with the early and late stage of infection, respectively. The changes in cell shape coincided with rearrangements of the cytoskeleton as well as with the cytoplasmic redistribution of mitochondria and late endosomes (see Figure 9 for a summary). Infection with the attenuated MVA did not induce any of these changes, demonstrating that they are not a virally induced artefact. MTs appeared to be the main player involved in the all of the early phenotypes, including the actin rearrangements (see below), as nocodazole treatment could either prevent or reverse them.

WtVV-induced MT changes were previously reported by Ploubidou *et al.* (25) to start at the onset of virus assembly. The MT rearrangements (bundling, de-organization and curling) described in that study clearly correspond to the 'early retraction phenotype' we observe, which starts as

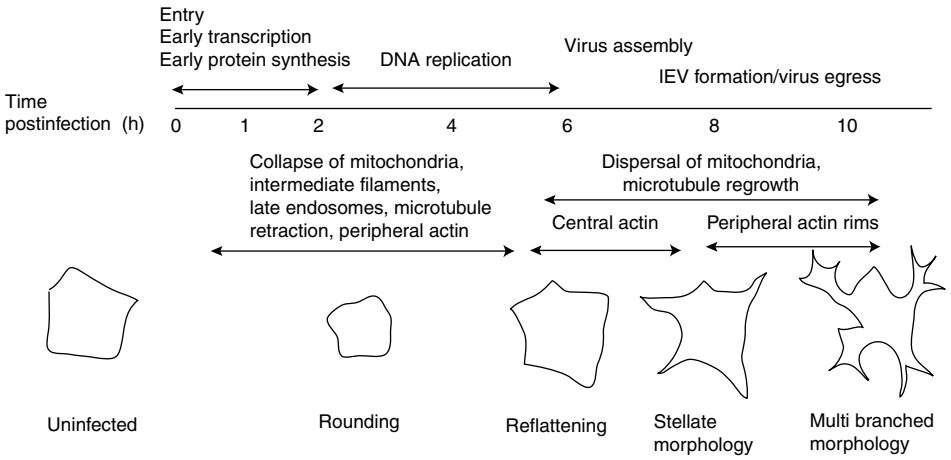

Figure 9: Summary of the cellular changes that occur during the course of VV infection. The horizontal line represents the times postinfection. The arrows above the line indicate the approximate start and duration of individual steps of VV morphogenesis. Below the line, the cellular changes, the approximate duration of which is indicated by the double arrows, are described that occur during the viral life cycle. Schematically shown are the cell-shape changes that appear sequentially during the course of the infection.

early as 1 h postinfection and depends on the synthesis of early proteins. The rearrangements originally described by Ploublidou *et al.* are difficult to reconcile with the rapid and efficient MT-dependent movement of IEVs to the cell surface late in infection (4). Our data now extend this study by showing that MTs first retract and then regrow into the cellular periphery late in infection concomitant with virus assembly and egress. That the late-MT changes allow the kinesin-dependent transport of IEVs towards the cellular periphery was supported by the fact that mitochondria and intermediate filaments that collapsed early in infection later regained (at least partially) their normal cytoplasmic distribution, strongly suggesting that (kinesin-mediated) transport along MTs was initially impaired and later restored. It is interesting to note that, in a related large DNA virus, African swine fever virus (ASFV), vimentin and mitochondria have also been shown to collapse around the nucleus (31,32), suggesting that this event may have benefits common to the organization of the cytoplasmic life cycles of both pox and ASF viruses.

In a separate study, we show that the early process of cell rounding coincides with the MT-dependent peri-nuclear accumulation of the cytoplasmic viral DNA-replication sites and may represent part of the driving forces for their inward movement (Schramm *et al.* in preparation). Thus, whereas cell rounding could drive the MT-dependent inward movement of the replication sites, cell reflattening may facilitate the MT- and actin-dependent egress of infectious particles late in infection.

It is intriguing that the rearrangements of the actin followed the virus life cycle in an even more precise manner (summarized in Figure 9). This network underwent subsequent changes that closely matched in time virus DNA replication (prominent peripheral actin rims), virus assembly (actin fibres crossing the entire cell) and egress (thin actin rims and actin tails). These phases also closely followed the cell-shape changes of cell rounding, reflattening and the multibranched morphology. All of actin phenotypes were, however, efficiently inhibited and reversed by nocodazole and thus the actin rearrangements depended on intact MTs. Given the major role of MTs in all of the observed cellular changes, it is surprising that nocodazole has only a moderate effect on the production of infectious progeny, at least *in vitro*. The production and egress of IEVs is, however, strictly dependent on intact MTs (25). In a previous study, Sanderson *et al.* argued that wtVV-induced cell rounding represents a transient phase that precedes wtVV-induced cell migration, a process that may also promote the spread of progeny *in vivo* (33). It is conceivable that one or more of the cellular phenotypes observed in the present study correspond to wtVV-induced cell motility. If true, our study strongly suggests that VV-induced motility may depend on intact MTs. As the processes of IEV egress and cell motility may both contribute significantly to virus spread *in vivo* and as both these processes may be depended on MTs, we suggest that *in vivo* MTs may play a crucial role in cell-to-cell spread required for efficient and successful poxvirus infection in animals and humans.

Cell rounding may present additional benefits

The clustering of organelles such as late endosomes and mitochondria around the nucleus could imply that outward MT-dependent transport, and thereby cellular secretion, may be impaired early in infection. It is conceivable that this disturbs the secretion of molecules that elicit an immune response and thus promotes the efficiency of virus production. It is intriguing that the collapse of late endosomes, a subset of which are known to be involved in antigen processing and presentation (34,35), was irreversible. Whereas this could imply that their cytoplasmic distribution is differently regulated compared with mitochondria or vimentin, it is also conceivable that this reflects a specific viral mechanism to inhibit antigen presentation. The fact that some of the cellular changes are only partially reversed late in infection could suggest that the amount of EEVs that are released from infected cells is to some extent inhibited. Such an inhibition could also support virus propagation, as EEVs are known to elicit neutralizing antibodies [reviewed in (36)]. The possibility that the EEV release may be controlled/inhibited during wtVV infection is supported by our recent study comparing MVA and wtVV infection in HeLa cells. Upon MVA infection in HeLa, IMV formation is blocked, and instead, immature (non-infectious) EEV-like particles are secreted from the cells. MVA secrets about three times more EEV-like particles from infected HeLa cells compared with EEV release following wtVV infection (37). We speculate that this difference could relate to the fact that MT-dependent transport may be unaffected upon MVA infection, leading to more secretion.

We propose that the reversible cell rounding may be beneficial for virus propagation in more than one way. The cellular changes are apparently not essential in cell culture, as, exemplified by the lack of these changes upon infection with MVA, they may be lost upon repeated passaging. Taken together, our synchronized infection study also strongly implies that processes of cell rounding and reflattening are intimately linked to distinct steps of the virus life cycle and thus may point to a sophisticated fine tuning of the way the virus has evolved to interact with its host.

Putative factors involved in the morphological changes

The early changes induced by wtVV infection are reminiscent of the over-expression/increased binding of MAPs, as previously suggested (25). The over-expression of the neuronal MAP tau in non-neuronal cells, for instance, has been shown to induce MT stabilization (38), cell rounding and the clustering of mitochondria and intermediate filaments around the nucleus (39). Similarly, over-expression of the ubiquitous MAP4 inhibits organelle motility, stabilizes MTs and results in a more peri-nuclear localization of

the endosomal recycling compartment (40,41). Thus, all of the VV-early phenotypes together, including the appearance of nocodazole-resistant MT pieces, suggest that increased MT binding of a MAP accounts, at least in part, for the early cellular changes. As the affinity of MAPs for MTs is known to be regulated by phosphorylation [see (42,43) and references therein], it is possible that wtVV modulates the binding of a cellular MAP using a virally encoded kinase/phosphatase or by viral proteins that regulate cellular kinases/phosphatases. However, the known viral kinases and phosphatase (H1R, F10L and B1R) are active in MVA, arguing for other players involved. An alternative possibility is thus that VV encodes for an early protein, missing in MVA, with affinity for MTs and/or MAP-like properties.

Increased MAP binding can, however, not explain how MTs retract from and subsequently regrow into the cellular periphery. This could suggest, rather than being stabilized, that MTs become more dynamic or that stabilization and a regulation of MT dynamics operate in parallel, perhaps on different subsets of MTs. The early retraction phenotype could suggest that, early in infection, peripheral MTs (those that obviously contact the peripheral actin fibres) undergo more shrinkage/catastrophe, whereas late in infection increased growth, and rescue is favoured leading to cell reflattening. Such a scenario is entirely consistent with the localization of EB1, showing that the dynamic plus ends of MTs are preferentially retracted early in infection but located at the leading edge of newly formed protrusion late in infection. Our data furthermore imply that MTs remain dynamically in contact with the cellular periphery, in particular the actin network, which was best exemplified by the fact that nocodazole entirely reversed/inhibited the actin rearrangements. Increasing evidence indicates that Rho GTPases, known for their ability to regulate actin dynamics also play an important role in regulating actin/MT interactions [reviewed in (44)]. The retraction and regrowth of MTs and the MT-dependent actin rearrangements that accompany the early and late stage of infection could underlie such a control, a hypothesis that we are currently testing. The fact that all of the observed phenotypes, in particular those affecting the MT and actin network, were not induced upon MVA infection provides a useful system to search for the molecules involved in the observed phenotypes. This search could also lead novel insights into the regulation of actin/MT interactions.

Materials and Methods

Cells, virus and antibodies

HeLa and BHK cells were essentially grown as described by Sodeik *et al.* (45). PtK2 cells were cultured in MEM containing 10% fetal calf serum. Sucrose-purified VV, strain WR (wtVV), was prepared as described by Jensen *et al.* (46). Purified MVA (clone F6, obtained from Dr Gerd Sutter; Paul-Ehrlich Institute, Frankfurt, Germany) was prepared in the same way, except that BHK cells were used for virus propagation. The following antibodies were used. Rabbit polyclonal antibodies to the wtVV genes H5R and A14L have been described (47,48). The mouse and rat monoclonal antibody to A27L (clone C3) and B5R (clone 19C2), respectively, were kind gifts of Mariano Esteban [CNB, Madrid, Spain (49)] and Gerhard Hiller (2). The monoclonal antibodies anti-α-tubulin and anti-vinculin were from Sigma (Hamburg, Germany), anti-vimentin V9 from Roche Biochemicals (Mannheim, Germany) and the monoclonal antibody to lamp-1 (clone H4A3) was from the Developmental Studies Hybridoma Bank (Iowa City, IA, USA). Monoclonal antibodies to $p150^{glued}$ were a kind gift of Walter Steffen (London, UK), and rabbit polyclonal to EB1, Clip-170 and α-tubulin were kindly provided by Eric Karsenti and Isabelle Vernos (EMBL, Heidelberg, Germany). To label mitochondria, we incubated cells for 30 min before fixing with 300 nM mitotracker (Molecular Probes; Karlsruhe, Germany). Actin was labelled with phalloidin coupled to rhodamine (Sigma) at 0.5 μg/mL and DNA with Hoechst (no. 33342 from Sigma) at 50 μg/mL. Anti-mouse or anti-rabbit coupled to fluorescein isothiocyanate or Cy3 was from Dianova (Hamburg, Germany).

Virus infections, indirect immunofluorescence

Purified virus preparations were titrated by immunofluorescence; cells grown on coverslips were infected with twofold dilutions of virus for 15 min at 37 °C, fixed at 3 h post-infection and labelled with anti-H5R (48) to visualize viral replication sites. The amount of virus resulting in an average of 10 replication sites per cell in approximately 95% of the cells was used throughout all experiments. This amount corresponds to a multiplicity of infection of approximately 60 (48).

For indirect immunofluorescence, the cells were seeded on 11-mm diameter coverslips a day before the infection. Infections were essentially done as described by Mallardo *et al.* (28) except that sucrose-purified virus was used. Briefly, cells were washed twice with serum-free DMEM (HeLa cells) or MEM (PtK2 cells) at 37 °C, equilibrated for 5–10 min in a CO_2 incubator at 37 °C. Meanwhile, virus was diluted in serum-free DMEM or MEM at 37 °C, briefly sonicated, added to the washed cells and incubated for 15–20 min at 37 °C in a CO_2 incubator. The cells were then washed three times with serum-free DMEM/MEM at 37 °C and incubated for the indicated times before fixing with either 3% paraformaldehyde in PBS at room temperature or methanol at −20 °C. This infection condition resulted in a synchronized infection (*Supplementary information 1* available online at http://www.blackwell-synergy.com).

Pre-extraction with Triton-X-100 before fixation was done as described by Mallardo *et al.* (50). Most image were taken with a Zeiss Axiovert 200M microscope equipped with 1.3 NA Plan Fluar × 40 or 1.4 Plan Apo Chromat × 63 lenses, an AxioCam camera (Zeiss) and acquisition software Axiovision (Zeiss). The images in Figures 1A–C, 2A–F, 3A–F and 4A–F were taken using a Zeiss LSM510 META confocal microscope, with a 1.4 Plan Apo Chromat × 63 lens. For infections performed in the presence of nocodazole, cells were placed in nocodazole containing media (20–30 μM) and incubated on ice for 1 h. Following another hour at 37 °C, the cells were infected as described and cultured in the presence of nocodazole until fixation. HU (5 mM working concentration) or CX (25 μg/mL working concentration) were added 15 min prior or immediately after infection to the respective cells. HU, CX and nocodazole were purchased from Sigma.

Quantification of light microscopy

For the determination of the cell size (defined as the surface occupied by the cell on the coverslip), pictures were taken with the Zeiss axiovert 200M using the × 63 lens. The area of the cell occupied on the coverslip was estimated using Image J program (downloadable free of charge from http://rsb.info.nih.gov/ij/) and was expressed as pixels. The cell borders were determined by DIC and by phalloidin staining and for the measurements the focal plane was used, in which the cell borders on the coverslip were readily discernible. The cell area occupied on the coverslip was drawn manually using the freehand selection tool of Image J. The pixel value of uninfected cells was taken as 100%, and the values obtained from infected cells expressed relative to the value obtained for uninfected cells. For each measurement, three different coverslips and 50–60 cells per coverslip were considered. To calculate the relative distribution of mitochondria or

vimentin, we drew the total cell surface area (defined as the area of the cell occupied on the coverslip) and the area occupied by the mitochondrial or anti-vimentin labelling manually, as for the determination of the cell size. The pixel value obtained for vimentin or mitochondrial labelling was then divided by the pixel value of the total cell surface, and the relative distribution was expressed as percentage of the total cell surface area. For each time point/condition, a minimum of 70 cells were considered. *T*-tests were applied to determine whether the observed differences were statistically relevant in the following way. For the cell size (Figure 1D,E), the relative size (expressed as a percentage relative to uninfected cells which was set as 100%) from three different experiments obtained from cells fixed at the indicated times postinfection was compared to uninfected cells which was set as 100%. p values smaller than 0.05 were considered statistically relevant. For the vimentin and mitochondria distribution (Figures 2G and 3G), the area occupied in the cell by mitotracker (mitochondria) or antibody labelling (vimentin) was compared. *T*-tests were applied to the labelled areas expressed in pixels of 70 uninfected versus 70 infected cells fixed at the indicated times postinfection. The p-values are listed in Supplementary information 3 (available online at http://www.blackwell-synergy.com).

Acknowledgments

We thank Trina Schroer for critical reading of the manuscript and for suggesting look at the cytoplasmic distribution of late endosomes. The members of the advanced light microscopy facility at the EMBL, Jens Rietdorf, Timo Zimmerman and Stephan Terjung, are acknowledged for their expert help and advice with the microscopes. This work was supported by an EMBO long-term fellowship to Birgit Schramm, a Marie Curie individual fellowship to CAMdH and a 5th framework EU network grant to Jacomine Krijnse Locker.

Supplementary Material

Supplementary information 1. The wtVV and MVA life cycle in HeLa and PtK2 cells.

Supplementary information 2. wtVV infection affects focal adhesion sites.

Supplementary information 3. p values for Figures 1–3.

References

1. Moss B. Poxviridae: the viruses and their replication, 4th edn. In: Fields BN, Knipe DM, Howley PM, Chanock RM, Hirsch MS, Melnick JL, Monath TP, Roizman B, editors. Fields Virology. Philadelphia, PA: Lippincott-Raven Press; 2001, pp. 2849–2883.
2. Schmelz M, Sodeik B, Ericsson M, Wolffe EJ, Shida H, Hiller G, Griffiths G. Assembly of vaccinia virus – the 2nd wrapping cisterna is derived from the trans-Golgi Network. J Virol 1994;68:130–147.
3. Tooze J, Hollinshead M, Reis B, Radsak K, Kern H. Progeny vaccinia and human cytomegalovirus particles utilize early endosomal cisternae for their envelopes. Eur J Cell Biol 1993;60:163–178.
4. Rietdorf J, Ploubidou A, Reckmann I, Holmstrom A, Frischknecht F, Zettl M, Zimmermann T, Way M. Kinesin-dependent movement on microtubules precedes actin-based motility of vaccinia virus. Nat Cell Biol 2001;3:992–1000.
5. Moss B, Ward BM. High-speed mass transit for poxviruses on microtubules. Nat Cell Biol 2001;3:E245–E246.
6. Carroll MW, Moss B. Host range and cytopathogenicity of the highly attenuated MVA strain of vaccinia virus: propagation and generation of recombinant viruses in a nonhuman mammalian cell line. Virology 1997;238:198–211.
7. Drexler I, Heller K, Wahren B, Erfle V, Sutter G. Highly attenuated modified vaccinia virus ankara replicates in baby hamster kidney cells, a potential host for virus propagation, but not in various human transformed and primary cells. J Gen Virol 1998;79:347–352.
8. Antoine G, Scheiflinger F, Dorner F, Falkner FG. The complete genomic sequence of the modified vaccinia Ankara strain: comparison with other orthopoxviruses. Virology 1998;244:365–396.
9. Ramirez JC, Gherardi M, Esteban M. Biology of attenuated modified vaccinia virus Ankara recombinant vector in mice: virus fate and activation of B- and T-cell immune responses in comparison with the western reserve strain and advantages as a vector. J Virol 2000;74:923–933.
10. Dorrell L, O'Callaghan CA, Britton W, Hambleton S, McMichael A, Smith GL, Rowland-Jones S, Blanchard TJ. Recombinant modified vaccinia virus Ankara efficiently restimulates human cytotoxic T lymphocytes in vitro. Vaccine 2000;15:327–336.
11. Belyakov IM, Earl P, Dzutsev A, Kuznetsov VA, Lemon M, Wyatt LS, Snyder JT, Ahlers JD, Franchini G, Moss B, Berzofsky JA. Shared modes of protection against poxvirus infection by attenuated and conventional smallpox vaccine viruses. Proc Natl Acad Sci USA 2003;100:9458–9463.
12. Earl PL, Americano JL, Wyatt LS, Eller LA, Whitbeck JC, Cohen GH et al. Immunogenicity of a highly attenuated MVA smallpox vaccine and protection against monkeypox. Nature 2004;428:182–185.
13. Andrade AA, Silva PNG, Pereira A, De Sousa LP, Ferreira PCP, Gazzinelli RT, Kroon EG, Ropert C, Bonjardim CA. The vaccinia virus-stimulated mitogen-activated protein kinase (MAPK) pathway is required for virus multiplication. Biochem J 2004;381:437–446.
14. Najarro P, Traktman P, Lewis JA. Vaccinia virus blocks gamma interferon signal transduction: viral VH1 phosphatase reverses Stat1 activation. J Virol 2001;75:3185–3196.
15. Everett H, McFadden G. Poxviruses and apoptosis: a time to die. Curr Opin Microbiol 2002;5:395–402.
16. Dobbelstein M, Shenk T. Protection against apoptosis by the vaccinia virus SPI-2 (B13R) gene product. J Virol 1996;70:6479–6485.
17. Smith GL. Vaccinia virus immune evasion. Immunol Lett 1999;65:55–62.
18. Shisler JL, Moss B. Immunology 102 at poxvirus U: avoiding apoptosis. Semin Immunol 2001;13:67–72.
19. Pedley S, Cooper RJ. The inhibition of Hela-cell RNA-synthesis following infection with vaccinia virus. J Gen Virol 1984;65:1687–1697.
20. Bablanian R, Esteban M, Baxt B, Sonnabend JA. Studies on mechanisms of vaccinia virus cytopathic effects.1. Inhibition of protein-synthesis in infected-cells is associated with virus-induced RNA-synthesis. J Gen Virol 1978;39:391–402.
21. Buller RM, Palumbo GJ. Poxvirus pathogenesis. Microbiol Rev 1991;55:80–122.
22. Meyer RK, Burger MM, Tschannen R, Schafer R. Actin filaments bundles in Vaccinia Virus infected fibroblasts. Arch Virol 1981;67:11–18.
23. Rottger S, Frischknecht F, Reckmann I, Smith GL, Way M. Interactions between vaccinia virus IEV membrane proteins and their roles in IEV assembly and actin tail formation. J Virol 1999;73:2863–2875.
24. Ferreira LRL, Moussatche N, Neto VM. Rearrangement of intermediate filament network of BHK-21 cells infected with vaccinia virus. Arch Virol 1994;138:273–285.
25. Ploubidou A, Moreau V, Ashman K, Reckmann I, Gonzalez C, Way M. Vaccinia virus infection disrupts microtubule organization and centrosome function. EMBO J 2000;19:3932–3944.
26. Sancho MC, Schleich S, Griffiths G, Krijnse-Locker J. The block in assembly of modified vaccinia virus Ankara in HeLa cells reveals new insights into vaccinia virus morphogenesis. J Virol 2002;76:8318–8334.
27. Gallego-Gomez JC, Risco C, Rodriguez D, Cabezas P, Guerra S, Carrascosa JL, Esteban M. Differences in virus-induced cell

morphology and in virus maturation between MVA and other strains (WR, Ankara, and NYCBH) of vaccinia virus in infected human cells. J Virol 2003;77:10606–10622.
28. Mallardo M, Leithe E, Schleich S, Roos N, Doglio L, Krijnse Locker J. On the relationship between intracellular cores, early mRNA and DNA-replication sites. J Virol 2002;76:5167–5183.
29. Schroer TA. Microtubules don and doff their caps: dynamic attachments at plus and minus ends. Curr Opin Cell Biol 2001;13: 92–96.
30. Schuyler SC, Pellman D. Microtubule 'plus-end-tracking proteins': the end is just the beginning. Cell 2001;105:421–424.
31. Rojo G, Chamorro M, Salas ML, Vinuela E, Cuezva JM, Salas J. Migration of mitochondria to the viral assembly sites in african swine fever virus-infected cells. J Virol 1998;72:7583–7588.
32. Heath CM, Windsor M, Wileman T. Aggresomes resemble sites specialized for virus assembly. J Cell Biol 2001;153:449–455.
33. Sanderson CM, Way M, Smith GL. Virus-induced cell motility. J Virol 1998;72:1235–1243.
34. Peters PJ, Raposo G, Neefjes JJ, Oorschot V, Leijendekker RL, Geuze HJ, Ploegh HL. Major histocompatibility complex class II compartments in human B lymphoblastoid cells are distinct from early endosomes. J Exp Med 1995;182:325–334.
35. Kleijmeer MJ, Morkowski S, Griffith JM, Rudensky AY, Geuze HJ. Major histocompatibility complex class II compartments in human and mouse B lymphoblasts represent conventional endocytic compartments. J Cell Biol 1997;139:639–649.
36. Smith GL, Vanderplasschen A, Law M. The formation and function of extracellular enveloped vaccinia virus. J Gen Virol 2002;83: 2915–2931.
37. Meiser A, Sancho C, Krijnse Locker J. Plasma membrane budding as an alternative release mechanism of the extracellular enveloped form of vaccinia virus from HeLa cells. J Virol 2003;77:9931–9942.
38. Lee G, Rook SL. Expression of tau protein in non-neuronal cells: microtubule binding and stabilization. J Cell Sci 1992;102:227–237.
39. Ebneth A, Godemann R, Stamer K, Illenberger S, Trinczek B, Mandelkow EM. Ovexrexpression of tau protein inhibits kinesin-dependent trafficking of vesicles, mitochondria, and endoplasmic reticulum-implications for Alzheimers-disease. J Cell Biol 1998;143:777–794.
40. Bulinski JC, McGraw TE, Guber D, Nguyen HL, Sheetz MP. Overexpression of MAP4 inhibits organelle motility and trafficking in vivo. J Cell Sci 1997;110:3055–3064.
41. Nguyen HL, Chari S, Gruber D, Lue C-M, Chapin SJ, Bulinski JC. Overexpression of full- or partial-length MAP4 stabilizes microtubules and alters cell growth. J Cell Sci 1997;110:281–294.
42. Chang W, Gruber D, Chari S, Kitazawa H, Hamazumi Y, Hisanaga S-I, Bulinski JC. Phosphorylation of MAP4 affects microtubule properties and cell cycle progression. J Cell Sci 2001;114:2879–2887.
43. Ebneth A, Drewes G, Mandelkow E-M, Mandelkow E. Phosphorylation of MAP2c and MAP4 by MARK kinases leads to the destabilization of microtubules in cells. Cell Mot Cyto 1999;44:209–224.
44. Watanabe T, Noritake J, Kaibuchi K. Regulation of microtubules in cell migration. Trends Cell Biol 2005;15:76–83.
45. Sodeik B, Doms RW, Ericsson M, Hiller G, Machamer CE, van ´t Hof W, van Meer G, Moss B, Griffiths G. Assembly of vaccinia virus – role of the intermediate compartment between the endoplasmic-reticulum and the Golgi stacks. J Cell Biol 1993;121:521–541.
46. Jensen ON, Houthaeve T, Shevchenko A, Cudmore S, Ashford T, Mann M, Griffiths G, Krijnse Locker J. Identification of the major membrane and core proteins of vaccinia virus by two-dimensional electrophoresis. J Virol 1996;70:7485–7497.
47. Salmons T, Kuhn A, Wylie F, Schleich S, Rodriguez JR, Rodriguez D, Esteban M, Griffiths G, Locker JK. Vaccinia virus membrane proteins p8 and p16 are co-translationally inserted into the rough ER and retained in the intermediate compartment. J Virol 1997;71:7404–7420.
48. Tolonen N, Doglio L, Schleich S, Krijnse Locker J. Vaccinia virus DNA replication occurs in endoplasmic reticulum-enclosed cytoplasmic mini-nuclei. Mol Biol Cell 2001;12:2031–2046.
49. Rodriguez JF, Paez E, Esteban M. A 14,000-Mr envelope protein of vaccinia virus is involved in cell fusion and forms covalently linked trimers. J Virol 1987;61:393–404.
50. Mallardo M, Schleich S, Krijnse Locker J. Microtubule-dependent organization of vaccinia virus core – derived early mRNAs into distinct cytoplasmic structures. Mol Biol Cell 2001;12:3875–3891.
51. Sodeik B, Cudmore S, Ericsson M, Esteban M, Niles EG, Griffiths G. Assembly of vaccinia virus: incorporation of p14 and p32 into the membrane of the intracellular mature virus. J Virol 1995;69:3560–3574.